Journal of Materials Chemistry B

Accepted Manuscript

ROYAL SOCIETY OF CHEMISTRY

www.rsc.org/materialsB

Magnetically guided survivin-siRNA delivery and simultaneous dual-modal imaging visualization based on Fe_3O_4@mTiO_2 nanospheres for breast cancer

Jiang Wu[a,1], Ying Liu[b,1], Wei Li[c], Chunyan Wang[b], Yanjun Li[b], Ying Tian[b], Jing Sun[b], Shouju Wang[b], Xin Wang[b], Yuxia Tang[b], Hong Zhu[a], Zhaogang Teng[b,*] and Guangming Lu[b,*]

[a] *Department of Nuclear Medicine, Jinling Hospital, School of Medicine, Nanjing University, Nanjing 210002, P.R. China*

[b] *Department of Medical Imaging, Jinling Hospital, School of Medicine, Nanjing University, Nanjing 210002, P.R. China*

[c] *Department of Chemistry, Shanghai Key Laboratory of Molecular Catalysis and Innovative Materials, and Laboratory of Advanced Materials, Fudan University, Shanghai 200433, P. R. China*

* Corresponding author. E-mail address: cjr.luguangming@vip.163.com; tzg@fudan.edu.cn; Fax: +86 25 8480 4659; Tel: +86 25 8086 0185

[1] These two authors contributed equally to this work.

Abstract: Small interfering RNA (siRNA) has great potential for gene therapy of breast cancer. The development of multifunctional nanocarriers possessing the targeted ability and multimodal imaging function is important to increase siRNA transfection efficiency and to visualize the delivery events. Herein, we demonstrate flavin mononucleotide (FMN) and polyethylenimine (PEI) modified Fe_3O_4@mTiO_2 nanoparticles (Fe_3O_4@mTiO_2/FMN-PEI) as a novel magnetic fluorescent siRNA delivery system. The system has magnetic targeting, magnetic resonance imaging (MRI), optical imaging, and high siRNA binding ability. Survivin-siRNA delivered by this system can effectively

enter into MCF-7 cells, which can be further enhanced by exerting an external magnetic field. More importantly, the siRNA delivery events including the location, trafficking, distribution, and release, can be visualized by MRI and optical imaging. Gene silencing by the survivin-siRNA can cause significant protein knockdown (96%) and considerable cell apoptosis (30%), indicating the usefulness of the Fe_3O_4@mTiO_2/FMN-PEI as a siRNA delivery system.

Keywords: Fe_3O_4@mTiO_2 nanospheres; Magnetic resonance imaging; Optical imaging; siRNA delivery; Breast cancer

1. Introduction

Breast cancer is the most common malignancy and the second leading cause of cancer death among women worldwide.[1] Surgery, chemotherapy, radiotherapy, endocrinotherapy, and molecular targeted therapy are the main methods for the management of breast cancer. However, these strategies are sometimes poorly effective or even ineffective; especially for advanced cases. Gene therapy, a novel approach, has shown a great potential to cure the genetic diseases including cancer.[2] As a promising gene therapy, RNA interference (RNAi) discovered by Fire et al. in 1998[3,4] can cause specific down-regulation of proteins through introduction of small interfering RNA (siRNA) to induce degradation of target mRNA. Survivin is the strongest anti-apoptotic factor of the inhibitors of apoptosis protein (IAP) family, which can inhibit cell apoptosis and is related to cell proliferation, angiogenesis, invasion, metastasis, resistance to therapy, and poor prognosis in breast cancer.[5-7] Thus, survivin-siRNA mediated down-regulation of the protein by survivin mRNA silencing can induce the apoptosis of breast cancer cells, which will further lead to the development of therapeutics.

It is known that siRNA itself is difficult to exert its silencing function owing to its intrinsic

deficiencies, such as short plasma half-life, poor membrane penetrability, and lack of targeting abilities.[8] For these reasons, a variety of vectors, including viruses, liposomes, polycations, and nanoparticles have been developed to transfer siRNA into the cytoplasm.[2] Among them, nanoparticles have attracted increasing attention as siRNA carriers because of their nanometer-scaled sizes, multi-functionality, facile surface modification, and low cost.[9-11] For instance, Katas et al. developed chitosan nanoparticles for safe and cost-effective siRNA delivery.[12] Sun and co-workers designed a siRNA delivery system through the self-assembled formation of micellar nanoparticles.[13] Nevertheless, there are still some challenges that need to overcome when these nanocarriers are used, such as how to increase transfection efficiency and visualize the delivery events. Magnetic magnetite (Fe_3O_4) nanoparticles have the special property of magnetic manipulation, which allows magnetic guidance for drug/gene targeted delivery and magnetic resonance imaging (MRI).[14-17] Thus, magnetic nanoparticle based siRNA delivery systems are very promising to increase transfection efficiency and to realize simultaneous visualization. Real-time and imaging-visible monitoring is especially crucial to gene therapy. Recently, some MRI-visible siRNA delivery vectors through polyethylenimine (PEI) coated iron oxide nanoparticles have been developed to obtain some important information during the process of gene therapy, such as the location and trafficking of siRNA.[18-20] However, the magnetic nanoparticles based MRI is difficult to monitor the intracellular distribution and release of siRNA due to the limit of spatial resolution.[21] Combining MRI with other imaging techniques such as optical imaging can offer a dual-modal imaging strategy and bring high sensitivity to subcellular visualization.[21-23] Thus, introducing optical information to magnetic nanocarriers may visualize the intracellular siRNA distribution, as well as the intracellular siRNA release from the vector, which is important to further exert its function. Currently, there are no

studies regarding optical/magnetic siRNA nanocarriers used for stimultaneous MRI and optical imaging.

To get multi-function, magnetic nanoparticles have been successfully modified by many inorganic and organic materials, such as silica, gold, and bovine serum albumin (BSA).[24-26] Mesoporous titanium dioxide (TiO_2) materials have been increasingly used in the biomedical field in recent years because of low cost, good biocompatibility, and facile surface modifications.[27-30] By utilization of the properties, mesoporous TiO_2 coated magnetite (Fe_3O_4@mTiO_2) are believed to be designed as a magnetic fluorescent carriers with high gene delivery efficiency and multimodal imaging capability. In this study, we prepared a novel siRNA delivery system based on flavin mononucleotide (FMN) and polyethylenimine (PEI) modified Fe_3O_4@mTiO_2 nanoparticles (Fe_3O_4@mTiO_2/FMN-PEI), which possessed magnetic targeting, MRI, optical imaging, and siRNA binding ability, due to the presence of Fe_3O_4 core, FMN (a fluorescent probe) attachment, and PEI coating. To the best of our knowledge, there is no report about using Fe_3O_4@mTiO_2 nanoparticles for siRNA delivery. *In vitro* experiments showed that survivin-siRNA delivered by this system was effectively phagocytized by breast cancer MCF-7 cells and magnetic guidance further increased their uptake. Moreover, some important siRNA delivery events such as the location, trafficking, and the intracellular distribution and release, were successfully visualized by MRI and optical imaging. Finally, 96% survivin protein knockdown and 30% cell apoptosis were confirmed by Western blot analysis and flow cytometry, which demonstrated the future promise of this siRNA delivery system.

2. Materials and methods

2.1 Materials

$FeCl_3 \cdot 6H_2O$, trisodium citrate, sodium acetate, ethylene glycol, ethanol, concentrated ammonia solution (28 wt%), and tetrabutyl titanate (TBOT) were of analytical grade and purchased from the Shanghai Chemical Corp (Shanghai, China). Riboflavin 5'-monophosphate, also known as flavin mononucleotide (FMN), was purchased from the Aladdin Company (Shanghai, China). Polyethyleneimine (PEI, branched, Mw 25000), DMSO and 3-(4, 5)-dimethylthiazol (-z-y1)-3, 5-di-phenytetrazoliumro-mide (MTT) were purchased from Sigma-Aldrich (Shanghai, China). DAPI and paraformaldehyde were provided by KeyGEN Biotech Co. Ltd (Jiangsu, China). Trypsins, fetal bovine serum (FBS), DMEM medium, Opti-MEM, and 0.05% trypsin-EDTA were provided by Gibco/ Life Technologies (Grand Island, New York, USA). The duplexed survivin-siRNA with or without a Cy5 fluorophore on the 5' end of the sense strand was purchased from Ribobio Co. Ltd (Guangzhou, China), according to the sequences of 5'-AAGCAUUCGUCCGGUUGCGCU-3', and 5'-AGCGCAACCGGACGAAUGCUU-3'. Diethypyrocarbonate (DEPC) water and Lipofectamine 2000 were purchased from Invitrogen Life Science (Shanghai, China). Agarose was purchased from Sangon Biotech Co. Ltd (Shanghai, China). TAE buffer was obtained from Beyotime Institute of Biotechnology (Jiangsu, China). GelRed was purchased from Biotium Inc. (Heyward, California, USA). Anti-survivin antibody was purchased from Abcam Company (Cambridge, UK). BSA was obtained from Amresco Company (Solon, Ohio, USA).

2.2 Preparation of Fe_3O_4@mTiO_2 (FT) nanospheres

The water-dispersible FT nanospheres were synthesized according to the method reported previously.[26] Typically, 3.25 g of $FeCl_3 \cdot 6H_2O$, 1.3 g of trisodium citrate, and 6.0 g of sodium acetate were dissolved in 100 mL of ethylene glycol. Then, the obtained solution was transferred into a Teflon-lined stainless-steel autoclave and heated at 200 ℃ for 10 h. After being allowed to cool to

room temperature, the obtained Fe_3O_4 nanoparticles were washed with ethanol for three times and dispersed in 100 mL of ethanol. Then, the Fe_3O_4 suspensions were mixed with concentrated ammonia aqueous solution (0.30 mL, 28 wt%) under ultrasound. After that, TBOT (0.75 mL) was added dropwise within 5 min. After stirring at 45 °C for 24 h, the FT nanospheres were washed with ethanol for three times and finally dried at 100 °C overnight.

2.3 Magnetic resonance imaging (MRI) of FT nanospheres

MRI was performed on a 3.0 T GE Discovery MR750, by using a T_2^* sequence (TR = 300 ms, TE = 2.19, 5.10, 8.02, 10.93, 13.84, 16.75, 19.66, and 22.58 ms; ETL: 16 k-space; flip angle = 25 deg; FOV = 120 mm; slice thickness = 2.5 mm; and image size = 256 × 256). The FT nanospheres were dissolved in 2 mL of water with five different concentrations (5, 10, 15, 20, 25 μg/mL). The corresponding iron concentrations were then determined by inductively coupled plasma (ICP) analysis by using a Perkin-Elmer Optima-5300DV spectrometer (Waltham, Massachusetts, USA). The obtained MR images of FT solutions were used to calculate the R_2^* values by using a GE AW Volume share 5 program (GE Healthcare/Greater China, Beijing, China). .

2.4 Preparation of Fe_3O_4@mTiO_2/FMN (FTF) and Fe_3O_4@mTiO_2/FMN-PEI (FTFP) nanospheres

The preparation of FTF nanoparticles was referred to the method that Wu et al. functionalized mesoporous titania nanoparticles with FMN.[29] Briefly, 1 mg of FMN powder was dissolved in 4 mL of water and then 10 mg of FT nanoparticles were added to the mixture. After stirring for 12 h, the mixed solution was centrifuged at 5500 rpms for 30 min and thoroughly washed with water. The obtained precipitate was dispersed in 2 mL water for further use.

To perform the PEI coating, 5 mg of as-prepared FTF nanoparticles were dispersed in 1 mL of

ethanol and then 1 mL of 2.5 mg/mL PEI ethanol solution was added dropwise. The mixed solution was sonicated and shaken for 30 min. The obtained product was washed with ethanol and water for three times, respectively.

2.5 Characterization of nanoparticles

The morphology and structure of the nanoparticles were characterized by transmission electron microscopy (TEM), which was performed on a JEOL JEM-2100 (HR) microscope (Jeol Inc., Tokyo, Japan) operated at 200 kV. Nitrogen sorption isotherms were measured using a Micromeritics Tristar 3000 analyzer at –196 °C. The sample was degassed at 180 °C for 10 h before the measurement. The Brunauer– Emmett–Teller (BET) method was utilized to calculate the specific surface area (SBET) using the adsorption data at p/p_0 = 0.05–0.15. The pore size distribution was derived from the adsorption branch by using the Barrett-Joyner-Halenda (BJH) model. The total pore volume (V_{total}) was estimated from the adsorbed amount at p/p_0 = 0.995. The hydrodynamic size and zeta potential of nanoparticles were measured using a Brookhaven analyzer (Brookhaven Instruments Co., Holtsville, New York, USA). Fourier transform infrared spectra (FTIR) were measured using a Nexus 870 spectrophotometer (Triad Scientific, Manasquan, New Jersey, USA). A Quantum Design MPMS-XL SQUID magnetometer (Quantum Design Inc., San Diego, California, USA) was used to determine the magnetic characteristics. Magnetization curves as a function of magnetic field were measured at 300 K under magnetic fields up to 20 kOe. Optical information of nanoparticles was obtained by performing fluorescence spectra by using a Fluoromax-4 Fluorescence Spectrometer (Horiba Scientific Inc., Edison, New Jersey, USA), as well as fluorescence imaging by using IVIS Lumina XR System (Xenogen Company, Alameda, California, USA).

2.6 Cell Culture and MTT cytotoxicity assay

The human breast adenocarcinoma cell line MCF-7 was obtained from American Type Culture Collection (ATCC). Cells were routinely grown in 25 cm^2 plastic culture flasks in DMEM medium containing 10% (v/v) FBS at 37 °C under a 5% CO_2 atmosphere with 95% relative humidity. The cellular toxicity was determined by MTT assay. MCF-7 cells were seeded in 96-well plates at a density of 1×10^4 cells per well. After 24 h of incubation, DMEM medium containing different FTFP concentrations from 5 to 100 μg/mL were added to the cell culture. After culturing for another 24 h and 48 h at 37 °C, MTT stock solution (10 μL, 5 mg/mL) was added into each well to incubate under cell culture for 4 h. After the removal of the supernatant, 100 μL of DMSO was added into each well to dissolve the resulting formazan crystals. Finally, the absorbance of each sample was measured with an automated microplate reader (BioTek, Winooski, Vermont, USA) at the wavelength of 570 nm. Cell viability was calculated by using the formula, absorbances (test cells)/absorbances (reference cells) × 100%.

2.7 Preparation of Fe_3O_4@mTiO_2/FMN-PEI-siRNA (FTFP-siRNA) nanoparticles and gel retardation assay

To bind siRNA, survivin-siRNA dry powder was dissolved with DEPC water and then was mixed with FTFP nanoparticles for 15 min at room temperature. To evaluate the siRNA binding ability of FTFP nanoparticles, a gel retardation assay was carried out by respectively mixing various weights of FTFP nanoparticles with 0.2 μg of survivin-siRNA at different weight ratios ranging from 1 to 64. After incubating 15 min, the resultant complexes were loaded onto 2% (w/v) agarose gel containing 0.01% (v/v) GelRed, and then were subjected to electrophoresis in TAE buffer at a constant voltage of 100 V for 20 min. Finally, the siRNA bands were visualized using a Tanon UV Gel Image System (Shanghai, China).

2.8 The delivery evaluation by confocal laser scanning microscopy

MCF-7 cells were seeded in five wells (5×10^4 per well) of a 24-well plate, which had coverslips in the bottom. After 24 h, the old medium was removed and the fresh medium without FBS and antibiotic was added into the five wells. Then, free survivin-siRNA^{Cy5}, Lipofectamine 2000-survivin-siRNA^{Cy5}, FTFP-survivin-siRNA^{Cy5} (weight ratio = 4), FTFP-survivin-siRNA^{Cy5} (weight ratio = 8), and FTFP-survivin-siRNA^{Cy5} (weight ratio = 8) with an external magnet were added into each well respectively. To prepare Lipofectamine 2000-survivin-siRNA^{Cy5}, Lipofectamine 2000 (1 μL) was diluted in 50 μL Opti-MEM for 5 min of incubation and then was mixed with 25 pmol (0.4 μg) survivin-siRNA^{Cy5} diluted in 50 μL Opti-MEM for 20 min at room temperature. To prepare FTFP-survivin-siRNA^{Cy5}, FTFP nanoparticles (1.6 and 3.2 μg) were respectively mixed with 25 pmol (0.4 μg) survivin-siRNA^{Cy5} for 15 min at room temperature. The final concentration of survivin-siRNA^{Cy5} was 25 nM in 1 mL culture medium of each well. After being incubated for 1 h, MCF-7 cells on coverslips were washed with PBS solution three times. Subsequently, they were fixed with 4% paraformaldehyde in PBS solution for 30 min and treated with DAPI (1.5 μg/mL in PBS solution) for 10 min in order to stain the nuclei. After that, coverslips loading MCF-7 cells were prepared to perform confocal laser scanning microscopy imaging using Olympus Fluoview FV10i (Olympus Instruments, Tokyo, Japan).

2.9 The delivery evaluation by magnetic resonance imaging (MRI)

MCF-7 cells were seeded in five cell culture dishes of 35 mm × 12 mm with 5×10^5 cells in 1.5 mL of DMEM medium in each dish. After attachment, the medium was removed and replaced with 1.5 mL of fresh medium without FBS and antibiotic. Then, MCF-7 cells in two dishes were respectively incubated with transfection solutions containing 40 and 80 μg FTFP, which had been combined with

survivin-siRNA at the weight ratio of 8 for 15 min. MCF-7 cells in the other two dishes were incubated with the same solutions, but had additional magnets under the dishes. Cells in the remaining dish were set as a control without any treatment. After 1 h at 37 °C, MCF-7 cells were rinsed with PBS solution three times and then digested with 0.05% trypsin-EDTA. The resulting cell pellets after centrifugation were dispersed with 1% (w/v) agarose solution. Then, the mixed solutions were transferred into a 2 mL Eppendorf tube for MRI. The agarose solution alone in an Eppendorf tube was set as the other control for imaging study. MRI methods were the same as described in section 2.3.

2.10 The delivery evaluation by inductively coupled plasma (ICP) analysis

First, 1.5 mL of DMEM medium containing approximate 15×10^4 MCF-7 cells were respectively added into three cell culture dishes of 35 mm × 12 mm. After 24 h of incubation, the mixed solution with 80 μg of FTFP and 10 μg of survivin-siRNA were respectively added into the two dishes with and without an external magnetic field. The remaining dish without any treatment was set as a blank. After culturing for another 1 h, the DMEM medium was removed and then the cells were washed with PBS buffer three times. Afterward, the MCF-7 cells were digested with 0.05% trypsin- EDTA and were harvested with centrifugation. The cells, then, were lysed with 300 μL of 95% HNO_3. After the solution turned achromic, 6 mL of water were added to dilute it. The intracellular concentration of titanium and iron in MCF-7 cells was quantitatively measured by using an inductively coupled plasma spectrometer (Perkin-Elmer Optima-5300DV, Waltham, Massachusetts, USA).

2.11 TUNEL assay

To confirm the effects of survivin-siRNA, a TUNEL assay was carried out to evaluate cell apoptosis caused by survivin protein knockdown. Lipofectamine 2000 was used as a carrier for survivin-siRNA

delivery. The MCF-7 cells were seeded at a concentration of 5×10^4 cells/mL in 96-well plates. After 24 h, the old medium was removed and 100 μL of Opti-MEM containing 1 μL of Lipofectamine 2000 and 40 pmol (0.64μg) of survivin-siRNA were added into the well. After 4 h of incubation, the transfection solution was discarded and replaced with the fresh DMEM with FBS for another 44 h. The cells in another well without any treatment were set as a control. Then, apoptosis was measured using the *in situ* cell death detection kit (Roche, Inc., Indianapolis, Indiana, USA) according to the manufacturer's instruction manual. Images from TUNEL-stained cells were captured with Olympus IX71 microscope (Olympus Instruments, Tokyo, Japan).

2.12 Western blot analysis

MCF-7 cells were seeded in two 6-well plates with 1×10^5 cells in 2 mL of DMEM medium per well. After attachment, the old medium was removed and replaced with transfection solution. FTFP-siRNA complexes were prepared by mixing 12.8 μg of FTFP nanospheres and 1.6 μg of survivin-siRNA (100 pmol) at the weight ratio of 8 for 15 min. To prepare the FTFP-siRNA transfection solution, the complexes were stabilized by 1 mg/mL BSA and then transferred into 2 mL of complete DMEM. Lipofectamine 2000-siRNA transfection solution was prepared according to the manufacturer's protocol. Briefly, 10 μL of Lipofectamine 2000 was diluted in 250 μL Opti-MEM for 5 min and then was mixed with 100 pmol survivin-siRNA diluted in 250 μL Opti-MEM for 20 min. After preparation, the FTFP nanospheres, FTFP-siRNA, and Lipofectamine 2000-siRNA were added into each well of a plate, respectively. The remaining well of the plate was set as a control without any treatment. FTFP-siRNA besides was added to a well with an external magnet under the other 6-well plate. The final concentration of survivin-siRNA is 50 nM in 2 mL culture medium of each well. After 4 h of incubation, the Lipofectamine 2000-siRNA transfection solution was discarded and

replaced with the fresh DMEM for another 68 h. After 12 h of incubation, FTFP-siRNA transfection solution was replaced with the fresh DMEM for another 60 h. After that, cells in each well were washed with cold PBS and lysed with a cell lysis buffer. Cells were then scraped and were under ultrasound for three times. After centrifugation at 4 ℃ for 15 min, protein extracts were obtained, which were then incubated in a sample buffer at 95 ℃ for 10 min. Afterward, the proteins were separated by gel electrophoresis on a 10% polyacrylamide gel containing SDS and then were blotted onto a polyvinylidene difluoride (PVDF) membrane according to a standard protocol. After blocking in 5% milk in Tris-buffered saline tween-20 (TBST) for 2 h, the membrane was incubated with primary antibody survivin (1:1000) and GAPDH (1:1000) overnight at 4 °C. After being washed with TBST three times, the membrane was incubated with a secondary antibody labeled with HRP for 2 h at room temperature. After the TBST was washed again, the signal of the membrane was detected by DAB coloration. ImageJ software was used to quantify image intensity.

2.13 Cell apoptosis analysis

MCF-7 cells were seeded in 24-well plates with 2.5×10^4 cells in 500 μL of DMEM medium per well. After attachment, the old medium was removed and Fe_3O_4@mTiO_2-PEI-siRNA transfection solution with or without an external magnet were added respectively. By mixing 3.2 μg of Fe_3O_4@mTiO_2-PEI nanospheres and 0.4 μg of survivin-siRNA (25 pmol) at the weight ratio of 8 for 15 min, the Fe_3O_4@mTiO_2-PEI-siRNA complexes were prepared. They were then stabilized by 1 mg/mL BSA before transferring into 500 μL of complete DMEM. The final concentration of survivin-siRNA is 50 nM each well. After 12 h of incubation, the transfection solution was replaced with the fresh DMEM for another 60 h. Cells without any treatment were set as a control. Subsequently, the cells were harvested and stained with Annexin V-FITC and PI by using an

Apoptosis Detection Kit (KeyGEN, Jiangsu, China) in accordance with the manufacturer's protocol. The rate of apoptosis was measured by a FASCalibur flow cytometer (Becton, Dickinson and Company, Franklin Lakes, New Jersey, USA).

3. Results and discussion

TEM images showed the obtained Fe_3O_4 (Fig. S1) and Fe_3O_4@mTiO_2 (Fig. 1a) nanoparticles possessed uniform spherical shape with average diameters of about 100 nm and 250 nm, respectively. Also, a core–shell structure was displayed for the Fe_3O_4@mTiO_2 nanoparticles and the TiO_2 layer coated on the magnetic particle had a thickness of approximately 70 nm (Fig. 1a). Nitrogen sorption isotherm of the Fe_3O_4@mTiO_2 nanoparticles showed a type IV curve with a hysteresis loop in the p/p_0 range of 0.4–0.6 (Fig. 1b), revealing characteristics of mesoporous materials. The surface area and pore volume were calculated to be 315.5 $m^2\ g^{-1}$ and 0.3 $cm^3\ g^{-1}$, respectively. The detailed pore size distribution revealed that the Fe_3O_4@mTiO_2 nanoparticles had uniform mesopores of about 2.5 nm (Fig. 1b, inset). The porous structure possessed by the Fe_3O_4@mTiO_2 nanoparticles provided abundant active sites to bind fluorescent FMN molecules through the strong interaction of phosphate ions of FMN with TiO_2 surfaces.[29] Magnetic characterization by using a magnetometer at 300 K indicated that the Fe_3O_4@mTiO_2 nanoparticles had a magnetization saturation value of 25 emu g^{-1} (Fig. 1c). Moreover, no hysteresis was observed on the magnetization curves, suggesting that the Fe_3O_4@mTiO_2 nanoparticles possessed the superparamagnetic character. Because of this, the nanoparticles can be designed as a MRI contrast medium for the visualization of siRNA delivery. The T_2^* enhancement capability of Fe_3O_4@mTiO_2 nanospheres was investigated by using a clinical 3.0 T MRI scanner. With the increase of iron concentration, the signal intensity of the measured

T_2^*-weighted image was gradually decreased (Fig. 1d). The corresponding R_2^* relaxivity of these nanospheres was quite high and gradually increased, indicative of the potential for T_2^*-weighted magnetic resonance imaging.

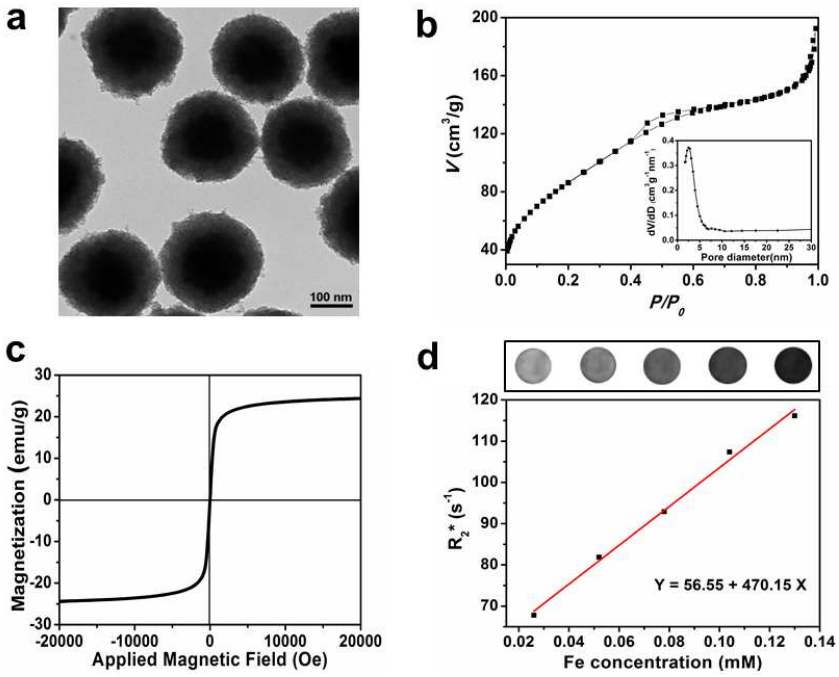

Fig. 1. (a) TEM image of Fe_3O_4@mTiO_2 nanospheres. (b) Nitrogen sorption isotherm and the inset pore size distribution curve of Fe_3O_4@mTiO_2 nanospheres. (c) Room-temperature magnetization curves of Fe_3O_4@mTiO_2 nanospheres. (d) T_2^*-weighted MR images and corresponding relaxation rate R_2^* of Fe_3O_4@mTiO_2 nanospheres of different Fe concentrations.

FTIR spectroscopy was carried out to characterize the conjunction of Fe_3O_4@mTiO_2 and FMN. As seen from Fig. 2a, the absorption peak of FT near 550 cm^{-1} is contributed from both Ti-O and Fe-O bonds.[31-33] The FTIR spectrum of FTF shows a new absorption peak at 1540 cm^{-1} compared to that of FT, which can be assigned to the stretching of C=N, indicative of successful FMN binding to FT through surface adsorption.[29,34] The coating of PEI was confirmed by increased C−H stretching

vibrations at 2924 cm^{-1} and 2847 cm^{-1}.[35,36] Also, the resulted FTFP nanoparticles expectedly showed strong excitation peaks at 410 and 430 nm according to fluorescence spectra (Fig. 2b). This suggests that FTFP can be used as a fluorescent probe. Simultaneously, fluorescence imaging demonstrated the presence of a fluorescence signal for FTF and FTFP (Fig. 2b, inset). In contrast, the FT nanoparticles showed the absence of that. In addition, the zeta potential and particle size of the nanoparticles were measured in aqueous solution. After the attachment of FMN to FT, the zeta potential value changes from -35.6 to -46.7 mV (Fig. 2c), due to abundant of negative phosphate groups in FMN. In strong contrast, the FTFP nanoparticles displayed a high positive zeta potential value of 37.1 mV (Fig. 2c). This suggested that cationic PEI molecules have been stably anchored on the surface of nanoparticles. The positive zeta potential makes the FTFP nanoparticles in favor of connection with siRNA and uptake by cells. The nanoparticle sizes of FT, FTF, and FTFP measured by dynamic light scattering (DLS) analysis were 285.9, 268.5, and 280 nm, respectively (Fig. 2d and Fig. S2). The results indicated that the surface modifications with FMN or PEI did not significantly change the particle size. Also, a smaller distribution breadth for FTFP nanoparticles was observed (Fig. 2d), which suggests the PEI coating slightly improves particle dispersion in water. TEM images also supported that surface modifications of FMN and PEI didn't change the structure of the nanoparticles (Fig. S3 and S4).

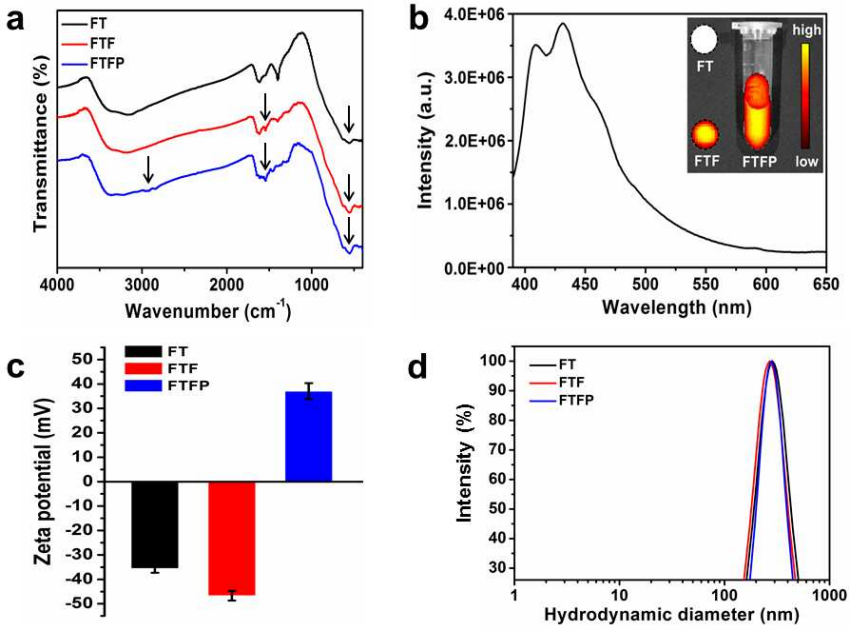

Fig. 2. (a) FTIR spectroscopy, (c) zeta potential and (d) hydrodynamic diameters of FT, FTF, FTFP nanospheres. (b) fluorescence spectra and fluorescence imaging (inset) of FTFP nanospheres.

The cytotoxicity of FTFP nanoparticles in the range of 5 to 100 μg/mL were evaluated by MTT assays. As shown in Fig. 3, there was no significant reduction of cell viability with the increase of FTFP concentration, for either the 24 or 48 h incubation period. Although the cell viabilities of the 48 h slightly decrease as compared to those of the 24 h, they all still exceed 85%. The MTT results indicated that FTFP can be used as a safe carrier for siRNA delivery.

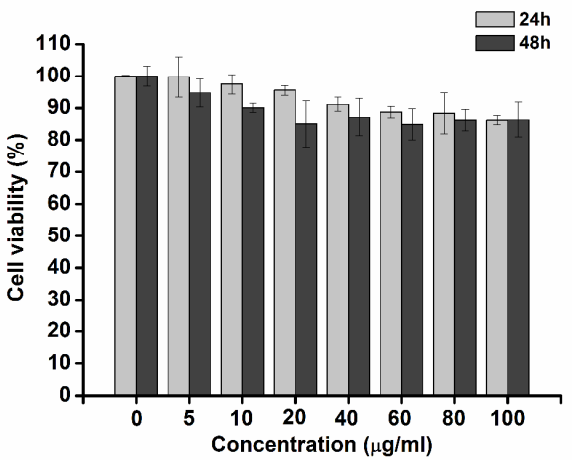

Fig. 3. Cytotoxicity of FTFP nanoparticles against MCF-7 cells for 24 h and 48 h at different concentrations.

Because of the electrostatic interaction between PEI and siRNA, the FTFP nanoparticles have the ability to bind siRNA, which was evaluated by a gel retardation assay. As shown in Fig. 4, free siRNA all appeared in the gel, indicating that the electrophoretic mobility of free siRNA was not inhibited at all. With increased weight ratios of FTFP to siRNA, the electrophoretic migration of siRNA was gradually retarded. When the weight ratio of FTFP to siRNA reached 8, the siRNA was extensively retarded and very few siRNA was revealed in the gel. The siRNA band in the gel fully disappeared at the weight ratio of 16, indicative of the absolute formation of FTFP-siRNA complexes. Meanwhile, the formation was also demonstrated by the complete retention of siRNA in the well. The gel retardation assay showed that the synthesized FTFP nanoparticles were capable of binding siRNA and were more efficient as compared with previously reported PEI-coating nanoparticles, which had the weight ratios (nanocarrier to siRNA) of more than 16 to completely bind siRNA.[24,37,38]

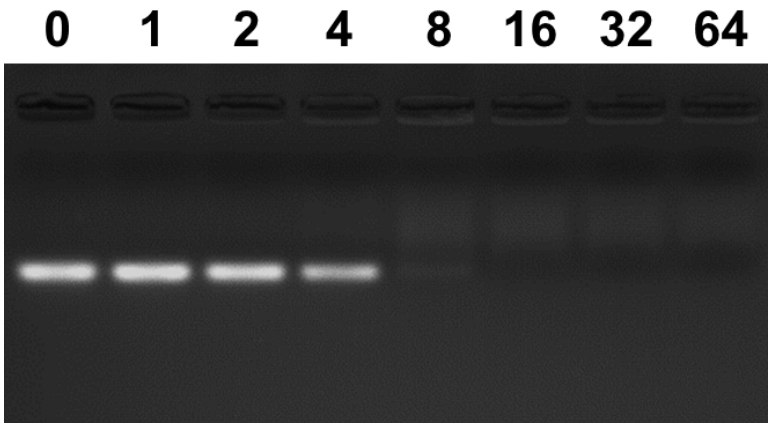

Fig. 4. Gel retardation assay of FTFP-siRNA nanoparticles. Lanes from left to right respectively represented the free siRNA (FTFP = 0) and different weight ratios (1, 2, 4, 8, 16, 32, 64) of FTFP nanoparticles to siRNA.

Confocal laser scanning microscopy was performed to evaluate FTFP-siRNA delivery into MCF-7 cells by the presence of Cy5-labeled siRNA (red) and FMN-bound FTFP (green). From Fig. 5a, it can be seen that free siRNA cannot enter MCF-7 cells because no red fluorescence is shown in them. This suggests the fact that the naked siRNA with negative charge was difficult to get access to the cell membrane. When using Lipofectamine 2000 as a transfection carrier, red fluorescence was observed in MCF-7 cells with 1 h of incubation, indicative of the intercellular siRNA distribution. In contrast to cells incubated with Lipofectamine 2000-siRNA, cells treated with FTFP-siRNA show green fluorescence and high red fluorescence, which indicated that FTFP-siRNA complexes had been distributed in cells and FTFP nanoparticles transfect siRNA more efficiently than Lipofectamine 2000 within 1 h of incubation. Compared with cells treated with FTFP-siRNA (weight ratio = 4), cells treated with FTFP-siRNA (weight ratio = 8) displayed higher red and green fluorescence intensity, indicative of a concentration-dependent delivery of FTFP-siRNA. Furthermore, MCF-7 cells treated with FTFP-siRNA (weight ratio = 8) under an external magnetic

field showed a drastically increased fluorescence intensity as compared to those without a magnet, indicative of its important role. In addition, merge images revealed yellow color representing co-localization of FTFP nanoparticles and siRNA, and red color representing the release of siRNA from FTFP nanoparticles (Fig. S5). The results of confocal laser scanning microscopy demonstrated that FTFP nanocarrier itself had the property of optical imaging, which visualized the higher delivery efficiency by magnetic guidance, as well as the intercellular siRNA distribution and the siRNA release from the vector.

Due to the fact that FT has a superparamagnetic character, the functionalized FTFP-siRNA was also explored as a contrast medium for MRI. In the T_2^*-weighted image (Fig. 5b), MCF-7 cells without any treatment presented a bright signal as similar as the agarose solution alone had. However, cells treated with FTFP-siRNA complexes for 1 h displayed a darker signal than cells without treatment. This indicated that the FTFP-siRNA complexes had entered into MCF-7 cells and the trafficking was visualized by MRI. Moreover, the signal intensity of MCF-7 cells was gradually low with the increase of FTFP-siRNA, which suggested that the delivery was in a concentration-dependent manner. Additionally, by exerting an external magnetic field, it lowers the signal intensity of MCF-7 cells incubated with transfection solutions containing 40 μg FTFP, as well as those containing 80 μg FTFP. Meanwhile, the corresponding R_2^* relaxivity of MCF-7 cells was also consistent with the T_2^* signal intensity as shown in Fig. 5b. The results demonstrated that FTFP based survivin-siRNA delivery system had the property of MRI, which visualized the location and trafficking of survivin-siRNA, and revealed the improved ability of FTFP-siRNA into MCF-7 cells after the magnetic guidance.

ICP analysis was further performed to confirm the delivery of FTFP-siRNA into MCF-7 cells.

Compared to the blank control without any treatment, cells with 1 h of incubation both showed significantly high concentration of titanium and iron (Fig. 5c). This demonstrated that FTFP-siRNA nanoparticles had been effectively phagocytized by MCF-7 cells. When a magnet field was exerted, the intracellular concentrations of titanium and iron were higher than those in cells without an external magnetic field. The results further demonstrated that an external magnet can improve the delivery of FTFP-siRNA into MCF-7 cells, due to the presence of a Fe_3O_4 core. On the basis of this, siRNA delivery through FTFP nanoparticles can be magnetically guided so as to improve siRNA delivery efficiency.

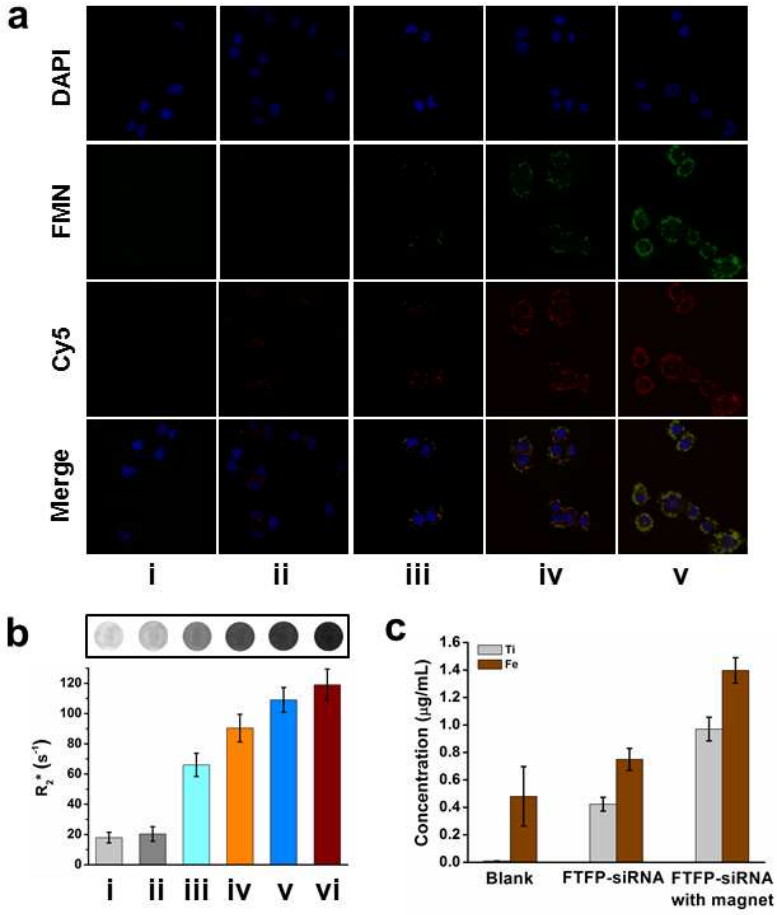

Fig. 5. (a) Confocal laser scanning microscopic images of MCF-7 cells incubated with free siRNA (i), Lipofectamine 2000-siRNA (ii), FTFP-siRNA (weight ratio = 4) (iii), FTFP-siRNA (weight ratio = 8)

(iv), and FTFP-siRNA (weight ratio = 8) under an external magnetic field (v) for 1 h. (b) MRI assessment of the delivery of FTFP-siRNA into MCF-7 cells, i ～ vi respectively representing agarose alone (i), MCF-cells without any treatment in agarose (ii), cells after incubation with 40 μg FTFP-siRNA in agarose (iii), cells after incubation with 40 μg FTFP-siRNA under an external magnetic field in agarose (iv), cells after incubation with 80 μg FTFP-siRNA in agarose (v), and cells after incubation with 80 μg FTFP-siRNA under an external magnetic field in agarose (vi). (c) Evaluation of the delivery of FTFP-siRNA into MCF-7 cells by ICP.

TUNEL assay showed many TUNEL-stained MCF-7 cells when using Lipofectamine 2000 to delivery survivin-siRNA, confirming that the siRNA was effective to induce cell apoptosis (Fig. 6a). The Western blot analysis was subsequently carried out to test the knockdown efficiency of FTFP-siRNA. As seen in Fig. 6b, there was almost no change between MCF-7 cells incubated with FTFP nanospheres and cells without any treatment, in regard to the survivin protein level. However, the level obviously decreased among MCF-7 cells respectively treated with Lipofectamine-siRNA, FTFP-siRNA, and FTFP-siRNA with an external magnet. These results demonstrated that survivin-siRNA delivered by FTFP nanoparticles as well as Lipofectamine 2000, effectively inhibited intracellular survivin protein expression through survivin gene silencing. According to the quantitative analysis resulting from ImageJ, the Lipofectamine-siRNA caused a 67% decrease of survivin protein level in MCF-7 cells. However, the level was suppressed by 83% when FTFP-siRNA was used. This indicated that FTFP-siRNA was more efficient than Lipofectamine-siRNA in knockdown of survivin protein due to the higher delivery efficiency as seen from confocal laser scanning microscopy. In addition, placing a magnet under cells expectedly

induced much higher knockdown efficiency of FTFP-siRNA with a 96% inhibition, which was well consistent with the delivery results assessed by confocal laser scanning microscopy, MRI, and ICP.

Survivin protein is closely related to cell division and apoptosis suppression. There have been lots of studies demonstrating that down-regulation of survivin protein can induce cell apoptosis in tumor cells.[39-44] To further investigate whether survivin-siRNA based on the delivery of FT nanoparticles induced apoptosis in MCF-7 cells, flow cytometry was performed. As shown in Fig. 6c, MCF-7 cells treated with Fe_3O_4@mTiO_2-PEI-siRNA transfection solution displayed 10% of early apoptosis and 14% of late apoptosis as compared with cells without any treatment showing 4% of apoptosis. Moreover, by having a magnetic field under cells a higher rate of apoptosis (total 30%) occurred. These results were in accordance with Western blot analysis, indicating that survivin-siRNA delivered by Fe_3O_4@mTiO_2-PEI nanoparticles into MCF-cells caused down-regulation of survivin protein by silencing the survivin gene, and further induced cell apoptosis so as to achieve the therapeutic purpose. Moreover, magnetic guidance enhanced these effects.

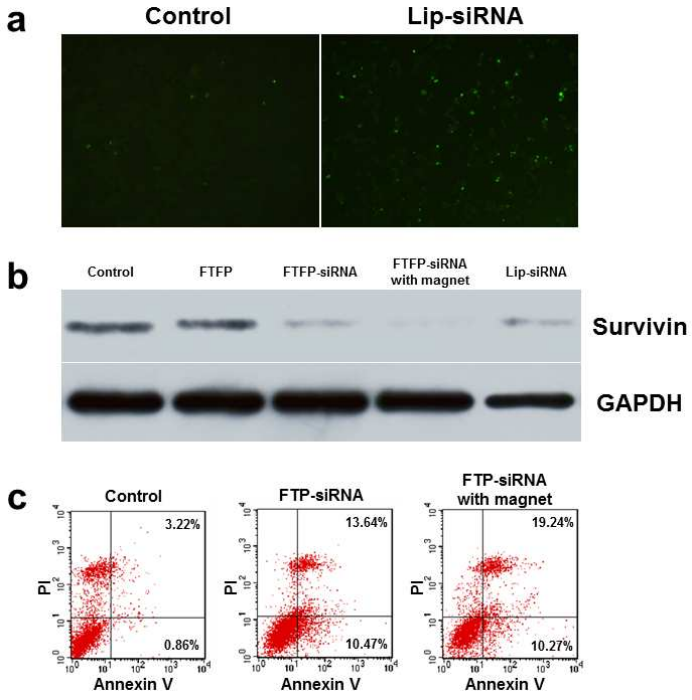

Fig. 6. (a) MCF-7 cells without any treatment (control) were rarely TUNEL-stained, but many of cells incubated with Lipofectamine 2000-siRNA were TUNEL-positive. (b) Western blot analysis showed Survivin and GAPDH (a control protein) expression, in MCF-7 cells without any treatment (control) and cells incubated with FTFP, FTFP-siRNA, FTFP-siRNA with an external magnet, and Lipofectamine 2000-siRNA, respectively. (c) Flow cytometry showed apoptosis in MCF-7 cells without any treatment (control), and cells incubated with Fe_3O_4@mTiO_2-PEI-siRNA (FTP-siRNA), FTP-siRNA with an external magnet.

4. Conclusion

In conclusion, this study has successfully prepared a novel dual-modal imaging-visible siRNA delivery system with high siRNA binding ability based on Fe_3O_4@mTiO_2/FMN-PEI nanoparticles. This system has a high siRNA transfection efficiency to breast cancer MCF-7 cells, which can get a further enhancement by a magnetic guidance. More importantly, the delivery events, including the location, trafficking, distribution, and release, can be visualized by MRI and optical imaging. Survivin-siRNA delivered by this system can cause significant knockdown of survivin protein and induce considerable cell apoptosis by gene silencing. Similarly, magnetic targeting can enhance survivin-siRNA silencing effects. Generally, this novel delivery system provides an important platform for safe and efficient siRNA delivery with magnetic targeted ability and dual-modal imaging visualization capability. In addition, due to the presence of the porous structure in the TiO_2 layer, this system in the future can be designed as a synergistic treatment platform by co-delivery of siRNA and chemotherapy drugs, which can be loaded in the pores.

Author contributions

Z.T. and G.L. conceived of and designed the experiments. J.W. wrote the manuscript. J.W. and Y.L. performed most of the experiments. W.L. and S.W. contributed to synthesize and characterize the nanoparticles. C.W. and X.W. contributed to the Western blot analysis. Y.L. and J.S. contributed to the MRI scan. Y.T. and Y.T. carried out confocal fluorescence microscopy imaging. Z.T. and H.Z. assisted with manuscript preparation.

Acknowledgements

We greatly appreciate financial support from the National Key Basic Research Program of the PRC (2014CB744504 and 2011CB707700), the Major International (Regional) Joint Research Program of China (81120108013), the National Natural Science Foundation of China (81201175, 81371611 and 81401469), the Natural Science Foundation of Jiangsu Province (BK20130863), and the National Science Foundation for Post-doctoral Scientists of China (2013T60939 and 2012M521934). We also express our sincere appreciation to Professor Morgan A. McClure, Department of Radiology, Nanchong Central hospital, for his linguistic modifications to this article.

References

1 R. Siegel, J. Ma, Z. Zou and A. Jemal, *CA-Cancer. J. Clin.*, 2014, **64**, 9-29.

2 L. Feng, X. Yang, X. Shi, X. Tan, R. Peng, J. Wang and Z. Liu, *Small*, 2013, **9**, 1989-1997.

3 Y. F. Tan, R. C. Mundargi, M. H. Chen, J. Lessig, B. Neu, S. S. Venkatraman and T. T. Wong, *Small*, 2014, **10**, 1790-1798.

4 Y. K. Buchman, E. Lellouche, S. Zigdon, M. Bechor, S. Michaeli and J. P. Lellouche,

Bioconjugate. Chem., 2013, **24**, 2076-2087.

5 K. Jha, M. Shukla and M. Pandey, *Surg. Oncol.*, 2012, **21**, 125-131.

6 G. Ambrosini, C. Adida and D. C. Altieri, *Nat. Med.*, 1997, **3**, 917-921.

7 J. Song, H. Su, Y. Y. Zhou and L. L. Guo, *Tumor. Biol.*, 2013, **34**, 2053-2062.

8 Y. Li, Q. Cheng, Q. Jiang, Y. Huang, H. Liu, Y. Zhao, W. Cao, G. Ma, F. Dai, X. Liang, Z. Liang and X. Zhang, *J. Control. Release*, 2014, **176**, 104-114.

9 Y. Shu, F. Pi, A. Sharma, M. Rajabi, F. Haque, D. Shu, M. Leggas, B. M. Evers and P. Guo, *Adv. Drug Delivery Rev.*, 2014, **66**, 74-89.

10 K. Y. Choi, O. F. Silvestre, X. L. Huang, K. H. Min, G. P. Howard, N. Hida, A. J. Jin, N. Carvajal, S. W. Lee, J. I. Hong and X. Y. Chen, *ACS Nano*, 2014, **8**, 4559-4570.

11 T. Devarasu, R. Saad, A. Ouadi, B. Frisch, E. Robinet, P. Laquerriere, J. C. Voegel, T. Baumert, J. Ogier and F. Meyer, *J. Mater. Chem. B*, 2013, **1**, 4692-4700.

12 H. Katas and H. O. Alpar, *J. Control. Release*, 2006, **115**, 216-225.

13 T. M. Sun, J. Z. Du, L. F. Yan, H. Q. Mao and J. Wang, *Biomaterials*, 2008, **29**, 4348-4355.

14 M. Ma, Y. Zhang, H. W. Gong, F. Q. Li and N. Gu, *J. Nanosci. Nanotechno.*, 2013, **13**, 6541-6545.

15 Z. H. Zhao, Z. J. Zhou, J. F. Bao, Z. Y. Wang, J. Hu, X. Q. Chi, K. Y. Ni, R. F. Wang, X. Y. Chen, Z. Chen and J. H. Gao, *Nat. Commun.*, 2013, **4**, 2266.

16 Z. X. Wu, W. Li, P. A. Webley and D. Y. Zhao, *Adv. Mater.*, 2012, **24**, 485-491.

17 Y. Liu, Y. Sun, C. Cao, Y. Yang, Y. Wu, D. Ju and F. Li, *Biomaterials*, 2014, **35**, 3348-3355.

18 Y. Chen, G. Lian, C. Liao, W. Wang, L. Zeng, C. Qian, K. Huang and X. Shuai, *J. Gastroenterol.*, 2013, **48**, 809-821.

19 X. Wang, Z. Zhou, Z. Wang, Y. Xue, Y. Zeng, J. Gao, L. Zhu, X. Zhang, G. Liu and X. Chen, *Nanoscale*, 2013, **5**, 8098-8104.

20 K. H. Bae, K. Lee, C. Kim and T. G. Park, *Biomaterials*, 2011, **32**, 176-184.

21 J. H. Lee, K. Lee, S. H. Moon, Y. Lee, T. G. Park and J. Cheon, *Angew. Chem. Int. Ed. Engl.*, 2009, **48**, 4174-4179.

22 R. Thomas, I. K. Park and Y. Y. Jeong, *Int. J. Mol. Sci.*, 2013, **14**, 15910-15930.

23 D. Pan, S. D. Caruthers, J. Chen, P. M. Winter, A. SenPan, A. H. Schmieder, S. A. Wickline and G. M. Lanza, *Future Med. Chem.*, 2010, **2**, 471-490.

24 L. Zhang, T. Wang, L. Li, C. Wang, Z. Su and J. Li, *Chem. Commun. (Camb.)*, 2012, **48**, 8706-8708.

25 L. Wang, J. Bai, Y. Li and Y. Huang, *Angew. Chem. Int. Ed. Engl.*, 2008, **47**, 2439-2442.

26 W. Li, J. Yang, Z. Wu, J. Wang, B. Li, S. Feng, Y. Deng, F. Zhang and D. Zhao, *J. Am. Chem. Soc*, 2012, **134**, 11864-11867.

27 P. J. Endres, T. Paunesku, S. Vogt, T. J. Meade and G. E. Woloschak, *J. Am. Chem. Soc.*, 2007, **129**, 15760-15761.

28 T. Paunesku, T. Rajh, G. Wiederrecht, J. Maser, S. Vogt, N. Stojicevic, M. Protic, B. Lai, J. Oryhon, M. Thurnauer and G. Woloschak, *Nat. Mater.*, 2003, **2**, 343-346.

29 K. C. Wu, Y. Yamauchi, C. Y. Hong, Y. H. Yang, Y. H. Liang, T. Funatsu and M. Tsunoda, *Chem. Commun. (Camb.)*, 2011, **47**, 5232-5234.

30 E. M. Brown, L. L. Allen, H. Pyles, J. Solis, T. A. Wileman and G. B. Willadsen, *J. Biomed. Nanotechnol.*, 2013, **9**, 539-550.

31 Y. Luo, Z. Lu, Y. Jiang, D. Wang, L. Yang, P. Huo, Z. Da, X. Bai, X. Xie and P. Yang, *Chem. Eng.*

J., 2014, **240**, 244-252.

32 F. He, F. Ma, J. Li, T. Li and G. Li, *Ceram. Int.*, 2014, **40**, 6441-6446.

33 P. Bhattacharya, G. Hatui, A. Mandal, C. K. Das, R. Kumar and T. C. Shami, *J. Alloy. Compd.*, 2014, **590**, 331-340.

34 K. Ariga, A. Kamino, H. Koyano and T. Kunitake, *J. Mater. Chem.*, 1997, **7**, 1155-1161.

35 S. Wang, Y. Zhou, H. Niu and X. Zhang, *Curr. Appl. Phys.*, 2011, **11**, 1337-1342.

36 M. Ratanajanchai, S. Soodvilai, N. Pimpha and P. Sunintaboon, *Mater. Sci. Eng. C Mater. Biol. Appl.*, 2014, **34**, 377-383.

37 K. H. Bae, K. Lee, C. Kim and T. G. Park, *Biomaterials*, 2011, **32**, 176-184.

38 H. Meng, M. Liong, T. Xia, Z. Li, Z. Ji, J. I. Zink and A. E. Nel, *ACS Nano*, 2010, **4**, 4539-4550.

39 Z. Xu, Z. Zhang, Y. Chen, L. Chen, L. Lin and Y. Li, *Biomaterials*, 2010, **31**, 916-922.

40 X. Q. Chen, S. Yang, Z. Y. Li, H. S. Lu, M. Q. Kang and T. Y. Lin, *Mol. Med. Rep.*, 2012, **5**, 917-922.

41 J. Shen, Q. Yin, L. Chen, Z. Zhang and Y. Li, *Biomaterials*, 2012, **33**, 8613-8624.

42 Y. Yang, Y. Gao, L. Chen, Y. Huang and Y. Li, *Int. J. Pharm.*, 2011, **405**, 188-195.

43 Q. Yin, J. Shen, L. Chen, Z. Zhang, W. Gu and Y. Li, *Biomaterials*, 2012, **33**, 6495-6506.

44 Q. Hu, W. Li, X. Hu, J. Shen, X. Jin, J. Zhou, G. Tang and P. K. Chu, *Biomaterials*, 2012, **33**, 6580-6591.

Graphical Abstract:

Magnetically guided survivin-siRNA delivery and simultaneous dual-modal imaging visualization based on Fe_3O_4@mTiO_2 nanospheres for breast cancer

Jiang Wu, Ying Liu, Wei Li, Chunyan Wang, Yanjun Li, Ying Tian, Jing Sun, Shouju Wang, Xin Wang, Yuxia Tang, Hong Zhu, Zhaogang Teng* and Guangming Lu*

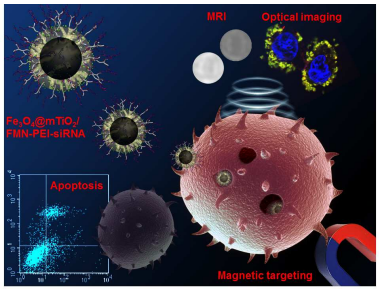

Fe_3O_4@mTiO_2/FMN-PEI as a siRNA delivery system can transfect survivin-siRNA to induce apoptosis, along with magnetic targeting, MRI and optical imaging.